

Dipole-Modulated Charge Transport through PNP-Type Single-Molecule Junctions

Mingyao Li,^{||} Huanyan Fu,^{||} Boyu Wang,^{||} Jie Cheng,^{||} Weilin Hu, Bing Yin, Peizhen Peng, Shuyao Zhou, Xike Gao,^{*} Chuancheng Jia,^{*} and Xuefeng Guo^{*}



Cite This: *J. Am. Chem. Soc.* 2022, 144, 20797–20803



Read Online

ACCESS |



Metrics & More

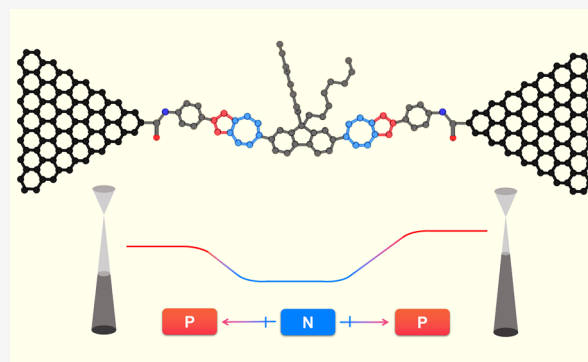


Article Recommendations



Supporting Information

ABSTRACT: The PNP structure realized by energy band engineering is widely used in various electronic and optoelectronic devices. In this work, we succeed in constructing a PNP-type single-molecule junction and explore the intrinsic characteristics of the PNP structure at the single-molecule level. A back-to-back azulene molecule is designed with opposite ~ 1.7 D dipole moments to create PNP-type single-molecule junctions. In combination with theoretical and experimental studies, it is found that the intrinsic dipole can effectively adjust single-molecule charge transport and the corresponding potential barriers. This energy band control and charge transport regulation at the single-molecule level improve deep understanding of molecular charge transport mechanisms and provide important insights into the development of high-performance functional molecular nanocircuits toward practical applications.



INTRODUCTION

Energy band engineering in electronic and optoelectronic devices is of great importance for the semiconductor industry, which can determine the function and performance of devices. In terms of macroscopic devices, many functional devices, such as bipolar junction transistors (BJTs) and field-effect transistors (FETs), can be constructed using appropriate energy bands to obtain high gain and an on–off switching ratio.^{1–8} The internal energy band structure of these devices is determined by the contact potential at the interface and space charge distribution, which has a great impact on device performance.^{9–15} There are mainly three methods to adjust the energy band in devices, including doping,¹⁶ lateral carrier injection,¹⁷ and longitudinal electric field.¹⁸ Through reasonably designing the chemical structure of a molecule or adjusting the chemical environment within the molecule, the energy band of a single molecule can also be adjusted, which regulates charge transport at the single-molecule level and continues device miniaturization according to Moore's law. For instance, by introducing different electronegative fragments into molecules, single-molecule PN junctions have been constructed to behave as rectifiers.^{19–21} By adjusting the energy band structure, single-molecule devices with special functions can be designed, which is of great significance for the study of the molecular property and the construction of high-performance nanoelectronic devices.

The PNP structure is an important structure constructed by energy band engineering, which is composed of an n-type

region sandwiched between two p-type regions. PN junctions on both sides lead to the formation of two back-to-back space charge regions with energy band bending. Since the transistor was proposed by the Bell laboratory in 1947,²² transistors having the PNP structure have been widely used in various electronic devices, such as BJT and FET. In addition, the PNP structure also widely exists in other molecular materials and devices, such as photodetectors.^{23–25} The single-molecule device platform provides an intrinsic way to study the PNP structure from the perspective of a single molecule. The energy band regulation has been effectively realized in single-molecule PN junctions. Similar models of P(N)–molecule–P(N) junctions with P(N)-doped semiconductor electrodes,^{26–28} by adjusting the molecule/electrode interface, can realize special heterojunction functions. The design of the molecule itself can provide more possibilities for adjusting the inherent electrical properties of single-molecule heterojunctions. The implementation of single-molecule PNP junctions will provide valuable insights into the molecular charge transport mechanisms and help design new single-molecule functional devices.

Received: August 15, 2022

Published: October 24, 2022



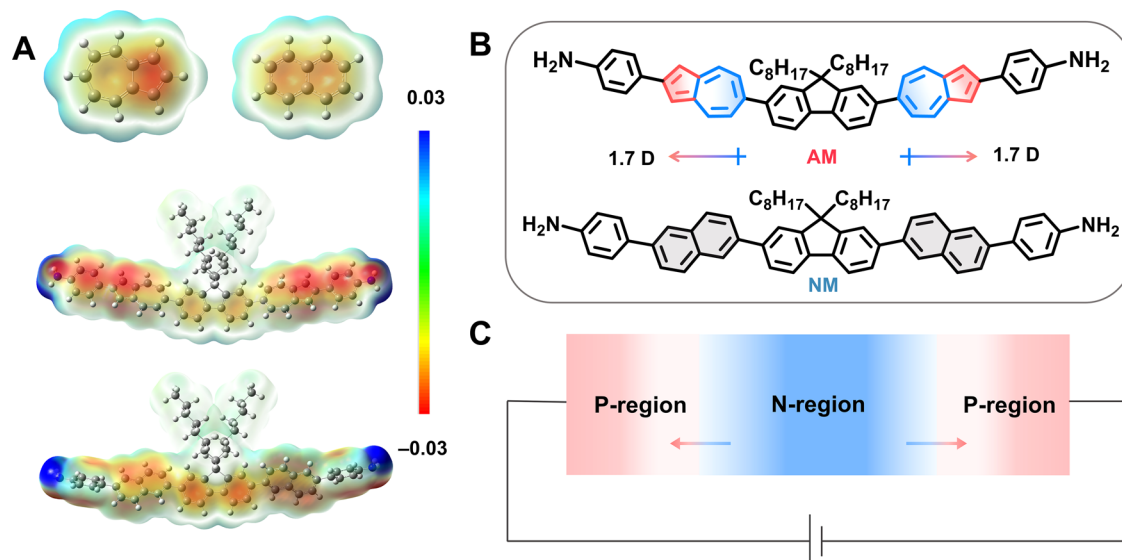


Figure 1. Design of the PNP-type molecule. (A) Calculated electrostatic potential mapping of the azulene unit (upper left), the naphthalene unit (upper right), the azulene molecule (middle), and the naphthalene molecule (down). Red color represents negative charge, while blue color represents positive charge. ESP unit: Hartree/e. (B) Structures of the designed azulene molecule (up) and the control naphthalene molecule (down). (C) Schematic diagram of the PNP structure in the circuit, where the arrows denote the directions of the dipole moment.

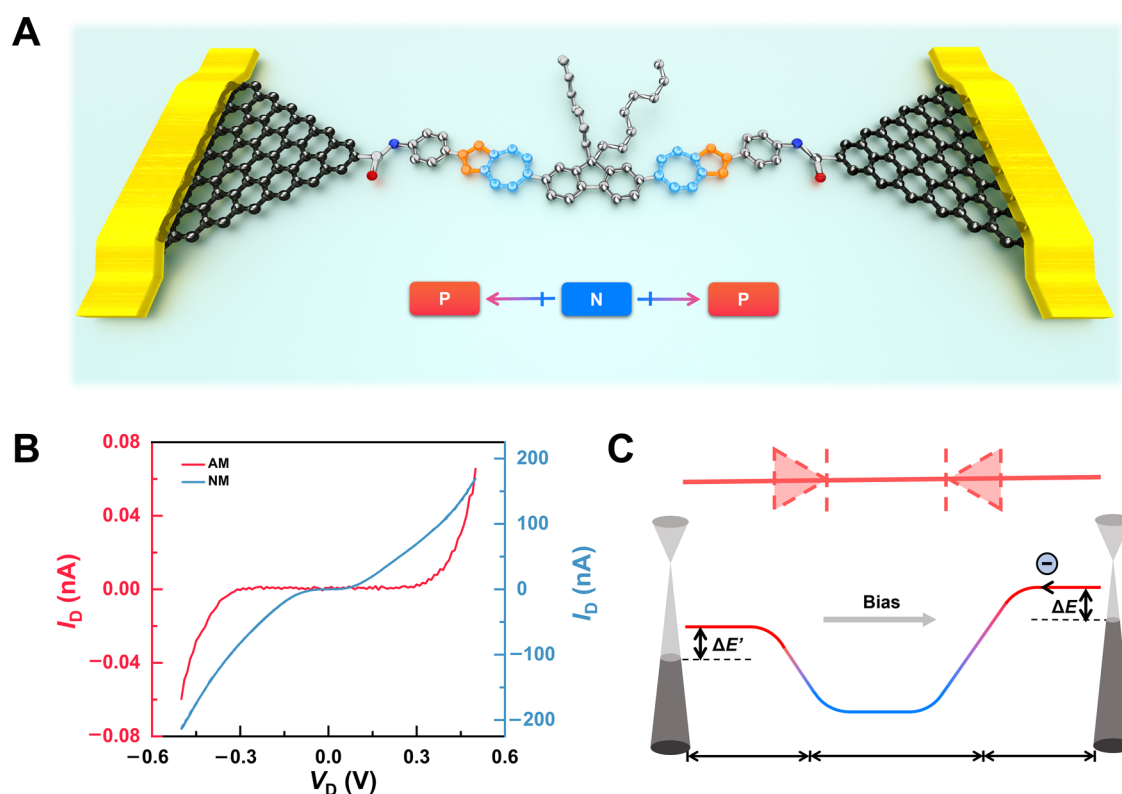


Figure 2. Construction of single-molecule devices. (A) Schematic diagram of the PNP-type single-molecule junction. (B) Current–voltage characteristics of the AM and NM devices at 5 K. (C) Schematic diagram of opposite diodes (up) and the energy band diagram for the PNP junction (down).

Azulene consists of a five-membered ring with a partially negative charge and a seven-membered ring with a partially positive charge. Owing to its inherent dipole moment, the azulene-based π -conjugation system has been used to construct various materials with unique properties, including conducting polymers, electrochromic materials, fluorescence switching materials, and anion receptors.^{29–33} In this work, the molecule

including two back-to-back azulene units was designed and used to construct single-molecule devices with the PNP structure. Meanwhile, naphthalene, as an isomer of azulene without dipole moment, served as the control. At low temperatures, the influence of the PNP structure on rectification was studied to clarify the intrinsic PNP properties. To explore the effect of the PNP structure on charge transport

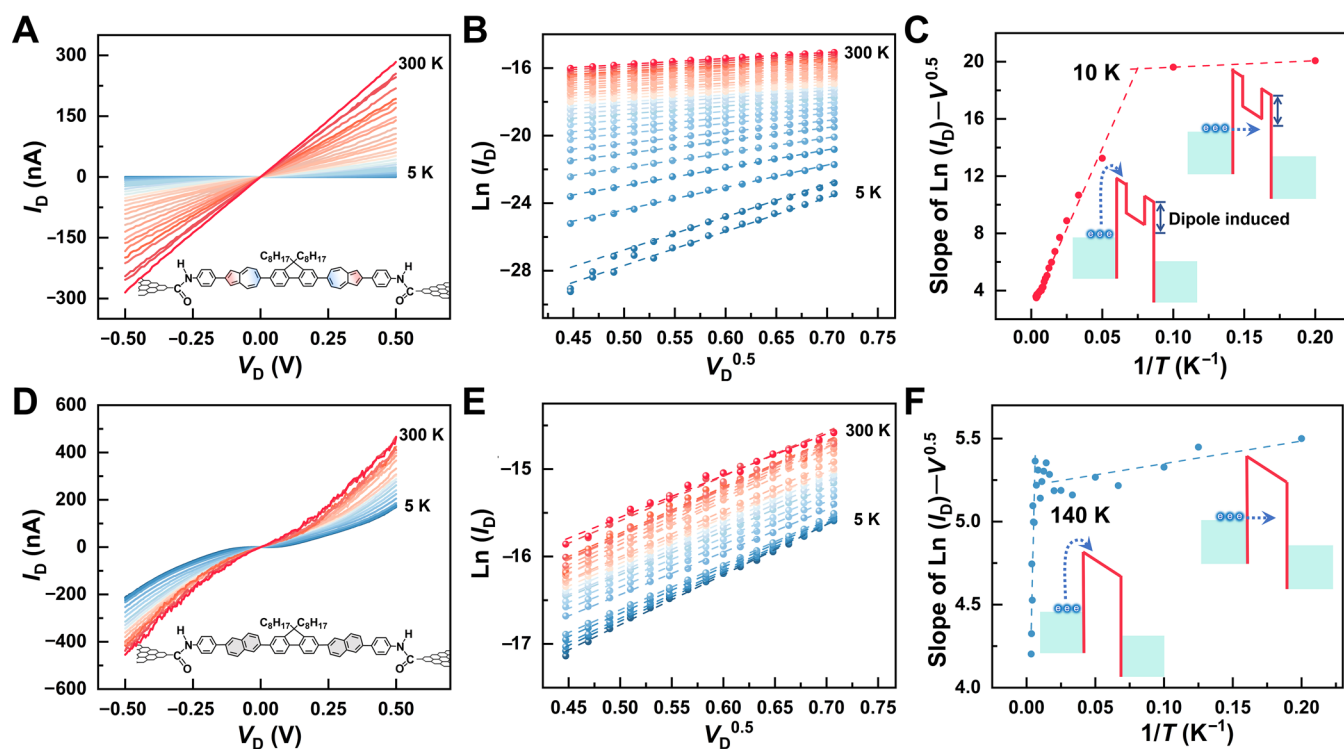


Figure 3. Temperature-dependent charge transport characteristics. (A, D) Temperature-dependent I – V curves for AM and NM, respectively. The insets show the corresponding structures of SMJs. (B, E) Plots of $\ln(I_b)$ vs $V_D^{0.5}$ at different temperatures for AM and NM, respectively. (C, F) Plots of the slope of $\ln(I_b) - V_D^{0.5}$ vs $1/T$ for AM and NM, respectively. The insets show the schematic diagram of barrier models at different temperatures.

characteristics, temperature-dependent charge transport investigations were conducted.

RESULTS AND DISCUSSION

Based on molecular engineering design, the PNP-type molecule based on azulene with a ~ 1.05 D dipole moment was synthesized, which has an energy band structure similar to that of PNP bipolar junctions (Figure 1). Specifically, the designed azulene molecule (AM) possesses two back-to-back azulene units with opposite dipole directions to form a PNP structure.³⁴ Through theoretical calculations, it was confirmed that AM possesses obvious charge separation. As shown in the calculated electrostatic potential, the inherent dipole moment on both sides is ~ 1.7 D (Figure 1A,B). The calculated electrostatic potential suggests that due to charge separation, the seven-membered ring of azulene becomes more positive and the five-membered ring becomes more negative. Similar to the charge distribution of the PN junction, the seven-membered ring is considered the N-region, while the other side is considered the P-region. The centrally locked diphenyl unit shows N-type characteristics due to its conjugation with two seven-membered rings. Therefore, the whole system offers a PNP-type single-molecule junction. As a control system, the naphthalene molecule (NM) containing two naphthalene units shows almost average charge distribution, and there is no net dipole moment along the molecular skeleton (Figure 1B). By comparing these two molecular systems, the influence of opposite dipole moments on charge transport of single-molecule devices could be explored.

To study the charge transport mechanism, the single PNP-type molecule and control molecule were connected into the circuit (Figures 2A, S1, and S3). Specifically, through a dashed-

line lithographic technology, graphene point electrode pairs with carboxyl end caps were fabricated using electron-beam lithography and plasma etching through a polymethylmethacrylate (PMMA) mask (Figure S2).³⁵ The AM and NM molecules with amino terminals were connected with the graphene point electrode pairs to form single-molecule junctions, respectively. The details of AM and NM syntheses and corresponding device fabrication are provided in Section 1 of the Supporting Information. The current–voltage (I – V) characteristics of the devices show that both molecules are successfully connected (Figure S4). The AM-based single-molecule junction (AM-SMJ) shows a lower conductance than the NM-based single-molecule junction (NM-SMJ) (Figure S4), especially at lower temperatures (Figure 2B). At the same time, when the temperature is low, the AM-SMJ has a higher turn-on voltage of ~ 0.3 V at both negative and positive sides, which indicates the bidirectional rectification properties at the negative and positive voltages, respectively. The bidirectional rectification means the rectification for both sides of PN junctions in the PNP structure due to the existence of potential barriers. It should be noted that the inherent two back-to-back rectifications in the molecule bring symmetry to the entire structure, resulting in symmetric I – V curves in Figure 2B. The decreased conductance and the extra turn-on voltage of the AM-SMJ can be well explained by the existence of double barriers generated by opposite double dipole moments. The double barriers are exerted along the molecule through the double dipole moments, which is similar to two diodes arranged in reverse (Figure 2C, up). These double barriers induced by the PNP structure suppress charge transport and generate extra turn-on voltage for activating charge transport, which reflects the regulation of single-molecule energy band

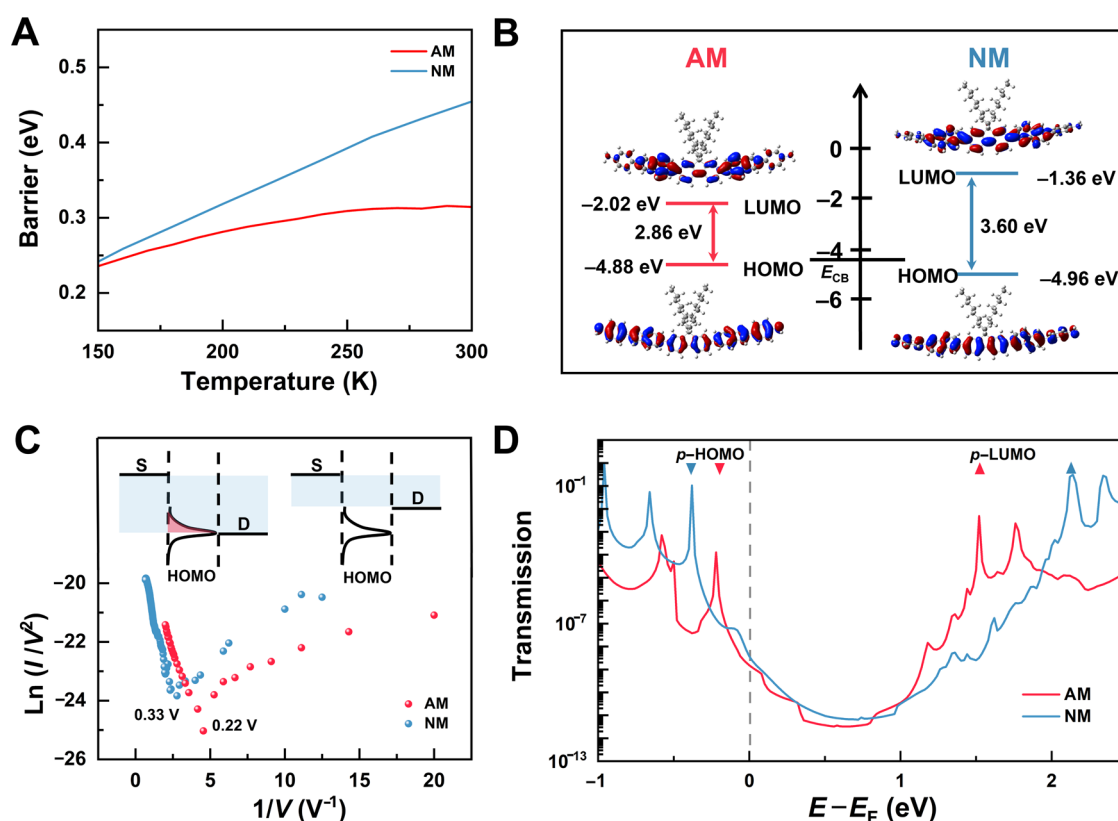


Figure 4. Energy-level-related transport mechanisms. (A) Thermal emission barrier of AM and NM. (B) Calculated molecular energy levels and related molecular orbital diagrams (HOMO and LUMO) of AM and NM. E_{CB} is the work function of graphene. (C) Plots of $\ln(I/V^2)$ vs $1/V$ of AM and NM. The insets show the corresponding charge transport model. (D) Zero-bias voltage transmission spectra of AM and NM. The p -HOMO and p -LUMO are marked with downward and upward triangles, respectively. The gray dashed line represents the Fermi level of graphene.

engineering. Interestingly, when electron carriers reversely transport through two diodes, the turn-on voltage corresponds to the reverse breakdown voltage. The turn-on voltage on both sides requires two diodes to be connected in opposite directions. The special double dipoles not only bring the double barriers but also modulate the energy band structure (Figure 2C, down). That is to say, different chemical environments along the molecule could generate charge distribution and band bending within the molecule.

The intrinsic charge transport properties of single-molecule devices can be defined from the temperature-dependent current–voltage (I – V) characteristics. The linearity or non-linearity of I – V curves may originate from the nature of molecules, such as the energy level of the dominant orbital and the molecular polarity. The current increases monotonously with temperature (Figure 3A,D), which implies a thermally activated transport mechanism. In the relatively high-temperature regime, the thermally activated conductance mechanisms for single-molecule junctions mainly include thermionic emission and hopping conductance. On the basis of the temperature-dependent I – V curves, the $\ln(I/V)$ is nonlinearly related to $1/T$ (Figure S5), and thus, the hopping mechanism is excluded.^{36,37} In contrast, the linear characteristics of plots $\ln(I)$ vs $V^{0.5}$ (Figure 3B,E) and the slope of $(\ln(I) \text{ vs } V^{0.5})$ vs $1/T$ (Figure 3C,F) indicate the thermionic emission mechanism.³⁸ In the relatively low-temperature regime, the dependence of charge transfer on temperature is weak, which indicates that the mechanism transitions from thermal emission to tunneling.^{39,40}

For the AM-SMJ, an obvious inflection point at ~ 10 K was observed from the slope of $(\ln(I) \text{ vs } V^{0.5})$ vs $1/T$ (Figure 3C), indicating that the charge transport mechanism has changed. In the high-temperature regime (>10 K), the transport characteristics of the PNP-type single-molecule junction fit well with the thermionic emission mechanism.⁴¹ According to the simple rigid band model, it suggests that in the process of charge transport, thermally excited electrons are injected from the electrode into the single molecule.⁴¹ In the low-temperature regime (<10 K), the energy of the electron is not enough to cross the barrier, so tunneling is the dominating transition mechanism. As for the NM-SMJ, it presents the situation of the original molecule without intramolecular dipole moment. The inflection point for the NM-SMJ from thermionic emission to tunneling is ~ 140 K (Figure 3F), which is similar to the traditional system,^{36,39} but much higher than that of the dipolar system. For the AM system, based on the aromaticity of Hückel's rule, charge separation between seven- and five-membered rings forms the intramolecular dipole. The energy required for dipole formation is ~ 1 meV (see Section 6.2 in the Supporting Information for details), which is consistent with the thermal energy of ~ 10 K. This indicates that the transition temperature of AM is related to the dipole moment, which is much lower than the traditional case.⁴² It is worth noting that three repetitive experiments showed consistent results of the transition temperature differences between AM and NM (Figures S6–S9).

Based on the simple rigid band model, the influence of dipole on the thermal emission barrier of the molecular junction is further analyzed. In the high-temperature regime

mentioned above, the I – V characteristics dominated by thermal emission can be explained by the Richardson–Schottky (RS) model. Specifically, electron carriers cross the potential barrier according to the thermionic emission mechanism, which can be modeled by the RS equation³⁸

$$I = AT^2 \exp\left(-\frac{q\Phi - q\sqrt{\frac{qV}{4\pi\epsilon_0\epsilon d}}}{kT}\right)$$

where A is the effective Richardson constant, ϵ_0 and ϵ are dielectric constants, q is the electron charge, d is the gap size between graphene electrodes, and Φ is the height of the thermal emission barrier.

It can be observed that the calculated thermal emission barrier of AM is about several hundred meV lower than that of NM (Figure 4A), and the slope is lower as well, which means that the dipole suppresses the barrier increase with the increase in temperature. The barrier analysis is also carried out according to the macroscopic PNP junction model (Figure S13), which is consistent with the barrier of thermal emission.⁴³ In addition, the thermal emission model shows a similar temperature-dependent trend (Figure 4A) with the macrosimulation (see Section 6.1 in the Supporting Information for details). The potential barrier increases with the increase in temperature, which can be attributed to the fact that the increase in temperature excites more electrons from the P-region to the N-region, thereby increasing the potential barrier of the energy band diagram.

As discussed above, the barrier height of the dipole-induced PNP system is lower than that of the control nondipolar system. The back-to-back dipole moment in AM could affect the barrier height. Here, the barrier generated by a single dipole in the PNP junction is theoretically analyzed, which has a dipole moment of ~ 1.7 D. The repulsive energy for the carrier is equal to the potential energy of the electron in the direction of the electrical dipole moment, and the electrical potential energy can be defined as⁴⁴

$$|V| = k\frac{P}{r^2}$$

where V is the electrical potential, k is the electrostatic constant, P is the dipole moment, and r is the distance between the dipole and the charge carrier injection site (~ 0.5 nm). Based on the above assumptions, the estimated extra electrical potential energy is about several hundred meV (see Section 6.3 in the Supporting Information for details), which matches the effect of the dipole moment on the height of the thermal emission barrier for AM. In addition, it is worth noting that the turn-on voltage (~ 300 mV) for the AM junction at low temperatures is the same as that of the dipole-induced barrier, indicating that the dipole plays a key role in charge transport.

The thermal emission barrier is generally reflected in the offset between the Fermi energy level of the electrode and the energy level of the adjacent conducting-dominated molecular orbital. The Fermi energy level of graphene electrodes is at ~ -4.6 eV, and the energy levels for HOMO of AM and NM are at ~ -4.88 and ~ -4.96 eV, respectively. The difference between them roughly corresponds to the potential barrier. According to the simple rigid band mode, the tunneling process can be analyzed by Fowler–Nordheim (F–N) plots of the I – V characteristics.³⁹ As described in Figure 4C, the

logarithmic dependence of $\ln(I/V^2)$ vs $1/V$ represents the direct tunneling in the low-bias regime, while in the high-bias regime, the linear dependence of the negative slope exhibits the F–N tunneling regime. The inflection points (V_{trans}) at ~ 0.22 and ~ 0.33 V can be obtained for AM and NM, respectively, which match the calculated molecular orbital diagrams of Figure 4B. A more rigorous charge transport model is based on resonant tunneling, which indicates that with the increase in bias voltage, the conducting molecular orbital enters the bias window, that is, from nonresonant tunneling to resonant tunneling, and the corresponding current increases significantly at the transition voltage. As shown in Figure 4D, since the HOMO of the molecule is closer to the Fermi level of the electrode (0 eV), the perturbed highest occupied molecular orbitals (p -HOMOs) of AM/NM dominate charge transport. The p -HOMO peak of AM is easier to access the bias window, which means that the corresponding inflection point appears at a smaller bias voltage. The results show that the dipole moment can regulate molecular orbitals and the corresponding energy bands. However, since the transmission spectrum of AM is lower than that of NM, especially for p -HOMO near the Fermi level, the conductance of AM is lower than that of NM, which is consistent with I – V curves shown in Figures 2 and 3.

CONCLUSIONS

In summary, a PNP-type single-molecule junction is constructed based on the back-to-back dipolar AM to simulate the energy band structure of macroscopic PNP junctions. At low temperatures, the bidirectional rectification properties are realized, which is consistent with the characteristics of the macrosystem. The internal dipole moment in the single-molecule PNP structure is found to effectively reduce the transport barrier and the transition temperature from thermionic emission to tunneling. Therefore, the single-molecule device can be used as an effective tool to study the charge transport characteristics of the PNP molecules. By controlling the inner charge distribution of the molecule, single-molecule PNP junctions can overcome important bottlenecks in the miniaturization of traditional semiconducting PNP junctions, such as the short channel effect and the drain-induced barrier-lowering effect, which are key to expanding Moore's law and promoting practical molecular electronics.

ASSOCIATED CONTENT

Supporting Information

The Supporting Information is available free of charge at <https://pubs.acs.org/doi/10.1021/jacs.2c08664>.

Schematic diagram of the graphene FET array and single-molecule junction fabrication process, I – V curves of single-molecule junctions, single-molecule connection statistics, theoretical analysis, electrical characterization, and barrier calculation (PDF)

AUTHOR INFORMATION

Corresponding Authors

Xike Gao – Key Laboratory of Synthetic and Self-Assembly Chemistry for Organic Functional Molecules, Shanghai Institute of Organic Chemistry, University of Chinese Academy of Sciences, Chinese Academy of Sciences, Shanghai 200032, P. R. China; orcid.org/0000-0003-2740-5529; Email: gaokx@mail.sioc.ac.cn

Chuancheng Jia – Beijing National Laboratory for Molecular Sciences, National Biomedical Imaging Center, College of Chemistry and Molecular Engineering, Peking University, Beijing 100871, P. R. China; Center of Single-Molecule Sciences, Institute of Modern Optics, Frontiers Science Center for New Organic Matter, Tianjin Key Laboratory of Micro-scale Optical Information Science and Technology, College of Electronic Information and Optical Engineering, Nankai University, Tianjin 300350, P. R. China; Email: jiacc@nankai.edu.cn

Xuefeng Guo – Beijing National Laboratory for Molecular Sciences, National Biomedical Imaging Center, College of Chemistry and Molecular Engineering, Peking University, Beijing 100871, P. R. China; Center of Single-Molecule Sciences, Institute of Modern Optics, Frontiers Science Center for New Organic Matter, Tianjin Key Laboratory of Micro-scale Optical Information Science and Technology, College of Electronic Information and Optical Engineering, Nankai University, Tianjin 300350, P. R. China; orcid.org/0000-0001-5723-8528; Email: guoxf@pku.edu.cn

Authors

Mingyao Li – Beijing National Laboratory for Molecular Sciences, National Biomedical Imaging Center, College of Chemistry and Molecular Engineering, Peking University, Beijing 100871, P. R. China

Huanyan Fu – Beijing National Laboratory for Molecular Sciences, National Biomedical Imaging Center, College of Chemistry and Molecular Engineering, Peking University, Beijing 100871, P. R. China; Center of Single-Molecule Sciences, Institute of Modern Optics, Frontiers Science Center for New Organic Matter, Tianjin Key Laboratory of Micro-scale Optical Information Science and Technology, College of Electronic Information and Optical Engineering, Nankai University, Tianjin 300350, P. R. China

Boyu Wang – Center of Single-Molecule Sciences, Institute of Modern Optics, Frontiers Science Center for New Organic Matter, Tianjin Key Laboratory of Micro-scale Optical Information Science and Technology, College of Electronic Information and Optical Engineering, Nankai University, Tianjin 300350, P. R. China

Jie Cheng – Key Laboratory of Synthetic and Self-Assembly Chemistry for Organic Functional Molecules, Shanghai Institute of Organic Chemistry, University of Chinese Academy of Sciences, Chinese Academy of Sciences, Shanghai 200032, P. R. China

Weilin Hu – Beijing National Laboratory for Molecular Sciences, National Biomedical Imaging Center, College of Chemistry and Molecular Engineering, Peking University, Beijing 100871, P. R. China

Bing Yin – Beijing National Laboratory for Molecular Sciences, National Biomedical Imaging Center, College of Chemistry and Molecular Engineering, Peking University, Beijing 100871, P. R. China

Peizhen Peng – Key Laboratory of Synthetic and Self-Assembly Chemistry for Organic Functional Molecules, Shanghai Institute of Organic Chemistry, University of Chinese Academy of Sciences, Chinese Academy of Sciences, Shanghai 200032, P. R. China

Shuyao Zhou – Beijing National Laboratory for Molecular Sciences, National Biomedical Imaging Center, College of Chemistry and Molecular Engineering, Peking University, Beijing 100871, P. R. China

Complete contact information is available at:

<https://pubs.acs.org/10.1021/jacs.2c08664>

Author Contributions

[†]M.L., H.F., B.W., and J.C. contributed equally to this work.

Notes

The authors declare no competing financial interest.

ACKNOWLEDGMENTS

The authors acknowledge primary financial support from the National Key R&D Program of China (2017YFA0204901, 2021YFA1200101, and 2021YFA1200102), the National Natural Science Foundation of China (22150013, 22173050, 21727806, and 22075310), the Tencent Foundation through the XPLOER PRIZE, the Fundamental Research Funds for the Central Universities (63223056), the “Frontiers Science Center for New Organic Matter” at Nankai University (63181206), the Natural Science Foundation of Beijing (2222009), and the Beijing National Laboratory for Molecular Sciences (BNLMS202105).

REFERENCES

- (1) Liu, L.; Xu, N.; Zhang, Y.; Zhao, P.; Chen, H.; Deng, S. Van der Waals bipolar junction transistor using vertically stacked two-dimensional atomic crystals. *Adv. Funct. Mater.* **2019**, *29*, No. 1807893.
- (2) Tybrandt, K.; Gabrielsson, E. O.; Berggren, M. Toward complementary ionic circuits: The npn ion bipolar junction transistor. *J. Am. Chem. Soc.* **2011**, *133*, 10141–10145.
- (3) Euvrard, J.; Rand, B. P. The advent of crystalline organic electronics. *Nature* **2022**, *606*, 661–662.
- (4) Lin, C.-Y.; Zhu, X.; Tsai, S.-H.; Tsai, S.-P.; Lei, S.; Shi, Y.; Li, L.-J.; Huang, S.-J.; Wu, W.-F.; Yeh, W.-K.; Su, Y.-K.; Wang, K. L.; Lan, Y.-W. Atomic-monolayer two-dimensional lateral quasi-heterojunction bipolar transistors with resonant tunneling phenomenon. *ACS Nano* **2017**, *11*, 11015–11023.
- (5) Yan, X.; Zhang, D. W.; Liu, C.; Bao, W.; Wang, S.; Ding, S.; Zheng, G.; Zhou, P. High performance amplifier element realization via MoS₂/GaTe heterostructures. *Adv. Sci.* **2018**, *5*, No. 1700830.
- (6) Paul Inbaraj, C. R.; Mathew, R. J.; Ulaganathan, R. K.; Sankar, R.; Kataria, M.; Lin, H. Y.; Chen, Y.-T.; Hofmann, M.; Lee, C.-H.; Chen, Y.-F. A bi-anti-ambipolar field effect transistor. *ACS Nano* **2021**, *15*, 8686–8693.
- (7) Liu, J.; Zhou, K.; Liu, J.; Zhu, J.; Zhen, Y.; Dong, H.; Hu, W. Organic-single-crystal vertical field-effect transistors and phototransistors. *Adv. Mater.* **2018**, *30*, No. 1803655.
- (8) Srisophon, S.; Jung, Y. S.; Kim, H. K. Metal-oxide-semiconductor field-effect transistor with a vacuum channel. *Nat. Nanotechnol.* **2012**, *7*, 504–508.
- (9) Rizzo, D. J.; Veber, G.; Cao, T.; Bronner, C.; Chen, T.; Zhao, F.; Rodriguez, H.; Louie, S. G.; Crommie, M. F.; Fischer, F. R. Topological band engineering of graphene nanoribbons. *Nature* **2018**, *560*, 204–208.
- (10) Wang, Y.; Zhang, R.; Chen, J.; Wu, H.; Lu, S.; Wang, K.; Li, H.; Harris, C. J.; Xi, K.; Kumar, R. V.; Ding, S. Enhancing catalytic activity of titanium oxide in lithium-sulfur batteries by band engineering. *Adv. Energy Mater.* **2019**, *9*, No. 1900953.
- (11) Huang, Z.; Wei, M.; Proppe, A. H.; Chen, H.; Chen, B.; Hou, Y.; Ning, Z.; Sargent, E. Band engineering via gradient molecular dopants for CsFA perovskite solar cells. *Adv. Funct. Mater.* **2021**, *31*, No. 2010572.
- (12) Ibáñez, M.; Hasler, R.; Genç, A.; Liu, Y.; Kuster, B.; Schuster, M.; Dobrozhan, O.; Cadavid, D.; Arbiol, J.; Cabot, A.; Kovalenko, M. V. Ligand-mediated band engineering in bottom-up assembled SnTe nanocomposites for thermoelectric energy conversion. *J. Am. Chem. Soc.* **2019**, *141*, 8025–8029.

- (13) Tan, G.; Zhao, L.-D.; Shi, F.; Doak, J. W.; Lo, S.-H.; Sun, H.; Wolverton, C.; Dravid, V. P.; Uher, C.; Kanatzidis, M. G. High thermoelectric performance of p-type SnTe via a synergistic band engineering and nanostructuring approach. *J. Am. Chem. Soc.* **2014**, *136*, 7006–7017.
- (14) Xie, C.; Zhang, X.; Wu, Y.; Zhang, X.; Zhang, X.; Wang, Y.; Zhang, W.; Gao, P.; Han, Y.; Jie, J. Surface passivation and band engineering: A way toward high efficiency graphene-planar Si solar cells. *J. Mater. Chem. A* **2013**, *1*, 8567–8574.
- (15) Zhang, P.; Wang, H.; Yan, D. Organic high electron mobility transistors realized by 2D electron gas. *Adv. Mater.* **2017**, *29*, No. 1702427.
- (16) Lee, F.; Tripathi, M.; Lynch, P.; Dalton, A. B. Configurational effects on strain and doping at graphene-silver nanowire interfaces. *Appl. Sci.* **2020**, *10*, 5157.
- (17) Mader, H.; Muller, R.; Beinvoogl, W. Bulk-barrier transistor. *IEEE Trans. Electron Devices* **1983**, *30*, 1380–1386.
- (18) Won, U. Y.; Ly, T. H.; Kim, Y. R.; Kang, W. T.; Shin, Y. S.; Lee, Ki Y.; Heo, J. S.; Kim, K. N.; Lee, Y. H.; Yu, W. J. Very high open-circuit voltage in dual-gate graphene/silicon heterojunction solar cells. *Nano Energy* **2018**, *53*, 398–404.
- (19) Xin, N.; Hu, C.; Al Sabea, H.; Zhang, M.; Zhou, C.; Meng, L.; Jia, C.; Gong, Y.; Li, Y.; Ke, G.; He, X.; Selvanathan, P.; Norel, L.; Ratner, M. A.; Liu, Z.; Xiao, S.; Rigaut, S.; Guo, H.; Guo, X. Tunable symmetry-breaking-induced dual functions in stable and photo-switched single-molecule junctions. *J. Am. Chem. Soc.* **2021**, *143*, 20811–20817.
- (20) Elbing, M.; Ochs, R.; Koentopp, M.; Fischer, M.; von Hänisch, C.; Weigend, F.; Evers, F.; Weber, H. B.; Mayor, M. A single-molecule diode. *Proc. Natl. Acad. Sci. U.S.A.* **2005**, *102*, 8815–8820.
- (21) Capozzi, B.; Xia, J.; Adak, O.; Dell, E. J.; Liu, Z.-F.; Taylor, J. C.; Neaton, J. B.; Campos, L. M.; Venkataraman, L. Single-molecule diodes with high rectification ratios through environmental control. *Nat. Nanotechnol.* **2015**, *10*, 522–527.
- (22) Bardeen, J.; Brattain, W. H. The transistor, a semi-conductor triode. *Phys. Rev.* **1948**, *74*, 230–231.
- (23) Kan, M.; Yang, C.; Wang, Q.; Zhang, Q.; Yan, Y.; Liu, K.; Guan, A.; Zheng, G. Defect-assisted electron tunneling for photo-electrochemical CO₂ reduction to ethanol at low overpotentials. *Adv. Energy Mater.* **2022**, *12*, No. 2201134.
- (24) Su, B.-W.; Zhang, X.-L.; Yao, B.-W.; Guo, H.-W.; Li, D.-K.; Chen, X.-D.; Liu, Z.-B.; Tian, J.-G. Laser writable multifunctional van der Waals heterostructures. *Small* **2020**, *16*, No. 2003593.
- (25) An, J.; Sun, T.; Wang, B.; Xu, J.; Li, S. Efficient graphene in-plane homogeneous p-n-p junction based infrared photodetectors with low dark current. *Sci. China Inf. Sci.* **2021**, *64*, No. 140403.
- (26) Peiris, C. R.; Ciampi, S.; Dief, E. M.; Zhang, J.; Canfield, P. J.; Le Brun, A. P.; Kosov, D. S.; Reimers, J. R.; Darwish, N. Spontaneous S–Si bonding of alkanethiols to Si(111)–H: towards Si–molecule–Si circuits. *Chem. Sci.* **2020**, *11*, 5246–5256.
- (27) Reimers, J. R.; Yang, J.; Darwish, N.; Kosov, D. S. Silicon–single molecule–silicon circuits. *Chem. Sci.* **2021**, *12*, 15870–15881.
- (28) Aragonès, A. C.; Darwish, N.; Ciampi, S.; Sanz, F.; Gooding, J. J.; Díez-Pérez, I. Single-molecule electrical contacts on silicon electrodes under ambient conditions. *Nat. Commun.* **2017**, *8*, No. 15056.
- (29) Tsurui, K.; Murai, M.; Ku, S.-Y.; Hawker, C. J.; Robb, M. J. Modulating the properties of azulene-containing polymers through controlled incorporation of regioisomers. *Adv. Funct. Mater.* **2014**, *24*, 7338–7347.
- (30) Xin, H.; Gao, X. Application of azulene in constructing organic optoelectronic materials: New tricks for an old dog. *ChemPlusChem* **2017**, *82*, 945–956.
- (31) Hou, I. C.; Berger, F.; Narita, A.; Müllen, K.; Hecht, S. Proton-gated ring-closure of a negative photochromic azulene-based diarylethene. *Angew. Chem., Int. Ed.* **2020**, *59*, 18532–18536.
- (32) Xin, H.; Hou, B.; Gao, X. Azulene-based π -functional materials: design, synthesis, and applications. *Acc. Chem. Res.* **2021**, *54*, 1737–1753.
- (33) Puodziukynaite, E.; Wang, H.-W.; Lawrence, J.; Wise, A. J.; Russell, T. P.; Barnes, M. D.; Emrick, T. Azulene methacrylate polymers: Synthesis, electronic properties, and solar cell fabrication. *J. Am. Chem. Soc.* **2014**, *136*, 11043–11049.
- (34) Fu, H.; Zhao, C.; Cheng, J.; Zhou, S.; Peng, P.; Hao, J.; Liu, Z.; Gao, X.; Jia, C.; Guo, X. Dipole-improved gating of azulene-based single-molecule transistors. *J. Mater. Chem. C* **2022**, *10*, 7803–7809.
- (35) Cao, Y.; Dong, S.; Liu, S.; He, L.; Gan, L.; Yu, X.; Steigerwald, M. L.; Wu, X.; Liu, Z.; Guo, X. Building high-throughput molecular junctions using indented graphene point contacts. *Angew. Chem., Int. Ed.* **2012**, *51*, 12228–12232.
- (36) Chen, X.; Jeon, Y.-M.; Jang, J.-W.; Qin, L.; Huo, F.; Wei, W.; Mirkin, C. A. On-wire lithography-generated molecule-based transport junctions: A new testbed for molecular electronics. *J. Am. Chem. Soc.* **2008**, *130*, 8166–8168.
- (37) Chen, J.; Calvet, L. C.; Reed, M. A.; Carr, D. W.; Grubisha, D. S.; Bennett, D. W. Electronic transport through metal-1,4-phenylene disocyanide-metal junctions. *Chem. Phys. Lett.* **1999**, *313*, 741–748.
- (38) Wang, W.; Lee, T.; Reed, M. A. Mechanism of electron conduction in self-assembled alkanethiol monolayer devices. *Phys. Rev. B* **2003**, *68*, No. 035416.
- (39) Sarker, B. K.; Khondaker, S. I. Thermionic emission and tunneling at carbon nanotube-organic semiconductor interface. *ACS Nano* **2012**, *6*, 4993–4999.
- (40) Araidai, M.; Tsukada, M. Theoretical calculations of electron transport in molecular junctions: Inflection behavior in Fowler-Nordheim plot and its origin. *Phys. Rev. B* **2010**, *81*, No. 235114.
- (41) Zhou, C.; Deshpande, M. R.; Reed, M. A.; Jones, L.; Tour, J. M. Nanoscale metal/self-assembled monolayer/metal heterostructures. *Appl. Phys. Lett.* **1997**, *71*, 611–613.
- (42) Kong, J. *A. Electromagnetic Wave Theory*, 1st ed.; EMW Publishing: Cambridge, MA, 2008; pp 309–319.
- (43) Sze, S. M. *Semiconductor Devices: Physics and Technology*, 2nd ed.; Wiley: New York, 2001; pp 72–73.
- (44) Vikramaditya, T.; Lin, S.-T. Novel donor-electret-acceptor framework for higher charge transfer and distance of charge transfer through dipole engineering. *J. Phys. Chem. C* **2021**, *125*, 20219–20229.